Biosensors and Bioelectronics 145 (2019) 111707

Contents lists available at ScienceDirect

Biosensors and Bioelectronics

journal homepage: www.elsevier.com/locate/bios

# Photoswitching enzymatic activity of horseradish peroxidase by graphene oxide for colorimetric immunoassay

Genxia Cao[1], Dongxue Sun[1], Tiantian Gu, Yuming Dong, Guang-Li Wang*

*International Joint Research Center for Photoresponsive Molecules and Materials, Key Laboratory of Synthetic and Biological Colloids (Ministry of Education), School of Chemical and Material Engineering, Jiangnan University, Wuxi, 214122, China*

ARTICLE INFO

*Keywords:*
Photoactivated enzyme
Horseradish peroxidase
Colorimetric immunoassay

ABSTRACT

In contrast to the conventional means that the activity of horseradish peroxidase (HRP) is initiated and terminated by the additives of peroxides and strongly acidic stop solutions, this study demonstrates that the enzymatic activity of HRP is switched through the visible light irradiated graphene oxide (GO). And this visible light driven activity of HRP can realize time-precise control without the aids of peroxides (typically $H_2O_2$) and acidic stop solutions. The superoxide anions ($O_2^{\bullet -}$) and photogenerated holes ($h^+$) produced by the photo irradiated GO are responsible for activating HRP and the subsequent oxidation of the typical substrates, i.e., 3, 3′, 5, 5′-tetramethylbenzidine (TMB) and 2, 2′-azino-bis(3-ethylbenzothiazoline-6-sulfonic acid) (ABTS). It is also validated that the photoswitchable HRP-GO mixture can act as an efficient signal reporter of bioassays by taking the sandwich immunoassay of alpha-fetoprotein (AFP) as an example. The AFP can be detected sensitively and selectively in the linear range from 0.2 fg/mL to 1.0 ng/mL, with a very low detection limit of 0.1 fg/mL. Advantages of the photoswitchable HRP-GO mixture include high catalytic ability, precise time control, and free of additionally harmful reagents.

## 1. Introduction

Enzyme based catalysts have been the hot spot in scientific community because of their fascinating characteristics, such as high activity, good specificity, as well as their widespread applications. Horseradish peroxidase (HRP), belonging to the family of heme enzymes for catalyzing the oxidation of a variety of substrates in the presence of peroxides, is one of the most popular and widely applied biocatalysts in various fields such as catalysis, organic synthesis, and, in particular, as reporters in various biosensors (Wen et al., 2011; Zhang et al., 2010; Xianyu et al., 2015). Conventionally, the activity of HRP is initiated and terminated through the addition of $H_2O_2$ and concentrated $H_2SO_4$ solution, respectively. However, the destructive and hazardous reagents ($H_2O_2$/concentrated $H_2SO_4$) used can not only cause irreversible denaturation of HRP but also are harmful to the operators and environment. As a result, to explore other alternative means to manipulate the activity of HRP remains an ongoing challenge.

It is proposed that photochemical control may be one of the solutions for the above problem (Bretschneider et al., 2010; Song et al., 2009; Kuwabata et al., 1994; Kamada et al., 2011). Interestingly, it has manifested that some nanomaterials such as CdS quantum dots (QDs) can trigger the catalytic activity of HRP for the oxidation of its fluorescent substrate (Amplex Ultrared) in aqueous solution under UV light irradiation even without the presence of the $H_2O_2$ (Fruk et al., 2007). The irradiated CdS QDs generated reactive oxygen species (mainly superoxide anion radicals and hydroxyl radicals), which triggered substrate oxidation by HRP. However, the excitation light (in the UV region) not only may result in photo- and/or thermal denaturation of the enzymes but also can bring about photodissolution of the used QDs. Lately, researchers also found that the activity of intercalated or adsorbed HRP can be easily initiated/terminated through UV or visible light irradiated iron-doped titanate (Kamada et al., 2011) or Pt-doped hematite (Kamada et al., 2012) solid layers. The generated holes by iron-doped titanate or Pt-doped hematite directly or indirectly oxidized HRP to its oxidation state (Compound I), and then the Compound I led to the oxidation of the organic substrate. Importantly, the visible light activated nanomaterial-HRP hybrid was found to possess outstanding durability because avoiding the irreversible photodenaturation of enzymes (Kamada et al., 2011, 2012). Recently, we demonstrated that the catechol compounds (such as catechol and dihydroxyphenylalanine) coordinated $TiO_2$ nanoparticles also stimulated the activity of HRP under visible light irradiation for oxidizing its chromogenic substrate of

* Corresponding author.
*E-mail address:* glwang@jiangnan.edu.cn (G.-L. Wang).
[1] These authors contribute equally to this work.

https://doi.org/10.1016/j.bios.2019.111707
Received 30 July 2019; Received in revised form 6 September 2019; Accepted 13 September 2019
Available online 16 September 2019
0956-5663/ © 2019 Elsevier B.V. All rights reserved.

3, 3′, 5, 5′-tetramethylbenzidine (TMB) (Wang et al., 2017; Li et al., 2018). All these researches indicate that combining photo irradiated nanomaterials with HRP may provide a green, facile and economic way to manipulate the activity of HRP, thus opening a new avenue for the applications of HRP. Unfortunately, up to now, the reported light-switchable nanomaterial-HRP systems are still rather constrained, not only resulted from the limited number of nanomaterials available to switch the activity of HRP under visible light, but also because of the undiversified biosensing applications.

Graphene oxide (GO) is attractive for various biological applications resulted from its excellent properties in terms of biocompatibility, low toxicity and high photostability against photobleaching and blinking (Asghar et al., 2019; Chung et al., 2013). Particularly, due to its versatile bandgap structure, recent studies have shown that the GO itself has excellent performances for initiating some photocatalytic reactions of small molecules, such as photocatalytic production of $H_2$ or/and $O_2$ (Yeh et al., 2010, 2011; Chen et al., 2016), conversion of $CO_2$ (Hsu et al., 2013), decomposition of organic pollutants (Krishnamoorthy et al., 2011) and so on. Recently, light irradiation was found to enhance the peroxidase-like activity of the $MoS_2$/GO hybrid through promoting electron transfer (Peng and Weng, 2017). However, no exploration has been made on the integration of GO with large biomolecules, such as natural enzymes, for photo induced biocatalysis.

Herein, we report the light-induced triggering of HRP activity using GO through the generation of superoxide anion radicals ($O_2^{\bullet -}$) and photogenerated holes ($h^+$). And the light triggered HRP-GO mixture can be utilized for the immunoassay of AFP with high sensitivity and good selectivity. Advantages of the bioinspired GO-HRP system include free of additionally harmful initiators/terminators, precise time controllability and high catalytic activity, which might open up new ways for generating light-switchable nanomaterial/enzyme hybrids applicable for biosensing or catalysis.

## 2. Experimental section

### 2.1. Materials and reagents

Superoxide dismutase (SOD) from bovine liver, catalase, horseradish peroxidase (HRP) and 2,2′-azino-bis(3-ethylbenzthiazolin-6-sulfonate) (ABTS) were purchased from Sigma-Aldrich (St. Louis, USA). 3,3′,5,5′-Tetramethylbenzidine (TMB), t–butanol, isopropanol, ethylene diamine tetraacetic acid (EDTA), potassium iodide (KI), graphite, $NaNO_3$, $KMnO_4$, 30% $H_2O_2$, $H_2SO_4$, and $HAuCl_4$ were obtained from Sinopharm Chemical Reagent Co., Ltd. (Shanghai, China). Avidin labeled HRP (Avidin–HRP) was purchased from Beyotime Biotechnology (Shanghai, China). Mouse-derived antihuman antibody pairs for human antigen AFP, carcinoembryonic antigen (CEA), prostate-specific antigen (PSA), and human IgG were purchased from Beijing Jorferin Bio-Technology Co., Ltd. (Beijing, China). All the DNA oligomers purified by HPLC were purchased from Sangon Biotechnology Co., Ltd. (Shanghai, China).

**Capture DNA ($C_{DNA}$)**: 5′-SH-$(CH_2)_6$-AAA AAA GAA GGA GGG GCG ACT-3′

**Biotin-$H_1$ (Biotin labeled hairpin $H_1$)**: 3′-CTT CCT CCC CGC TGA CAA AGT TCA GCG GGG-biotin-5′

**Biotin-$H_2$ (Biotin labeled hairpin $H_2$)**: 5′-biotin-GTT TCA AGT CGC CCC GAA GGA GGG GCG ACT-3′

The underlined parts of the sequences indicate the sticky ends.

### 2.2. Apparatus

Fourier transform infrared (FT–IR) spectrum was recorded on a Nicolet FT–IR 6700 spectrometer (ThermoFisher, USA) under room temperature and under dry condition by potassium bromide pellet technique. Raman spectra were recorded on a confocal Raman spectrometer (Renishaw, Britain) with 532 nm laser excitation at room temperature. A JEOL JEM-2100 transmission electron microscope (Hitachi, Japan) was utilized to characterize the morphology of GO under room temperature. X-ray diffraction (XRD) measurement was carried out at room temperature on D8 X-ray powder diffractometer (Brooke AXS, Germany) with Cu Kα radiation ($\lambda = 0.154178$ nm) and a scanning speed of 4°/min within the scope of 2–60°. UV–vis absorption spectroscopic measurements were carried out using a TU–1901 spectrophotometer (Beijing Purkinje General Instrument Co., Ltd., China). A 300 W Xe lamp (NBeT, China) equipped with an ultraviolet cutoff filter ($\lambda \geq 400$ nm) was used as the irradiation source. The detection of AFP by the absorption method was conducted using a SpectraMax M5 microplate reader (Molecular Devices, USA).

### 2.3. Preparation of GO

GO was prepared from natural graphite powder through a modified Hummers' method (Hummers and Offeman, 1958). In a typical synthesis, 0.5 g of graphite and 0.5 g $NaNO_3$ were added into 16.5 mL of 98% $H_2SO_4$ (under ice bath), followed by stirring for about 24 h at room temperature. Subsequently, the mixture was kept at 0 °C in an ice bath, followed by the slow addition of 3.0 g $KMnO_4$ and stirred for 1 h. Then, the mixture was heated to 35–40 °C and stirred for another 30 min. After the addition of 40 mL of ultrapure water, the temperature of the mixture was raised to around 98 °C, and then 460 mL of water was added during a period of 15 min. Finally, 1400 mL of water and 100 mL of 30% $H_2O_2$ were added into the mixture to stop the reaction. After the product was collected by filter flask and washed repeatedly with 5% HCl aqueous solution. The product was allowed to dry at 50 °C in a vacuum drying apparatus.

The GO synthesized by the above method can be dispersed in water easily. A 1.0 mg of the GO powder was dispersed in 20 mL ultrapure water with the aid of ultrasonication to form a homogeneous solution (0.05 mg/mL).

### 2.4. Triggering the activity of HRP by the photo irradiated GO

We employed TMB and ABTS as two substrates to measure the photo induced catalytic activity of GO alone and the HRP-GO mixture in our experiments. Specifically, 100 μL of GO (0.05 mg/mL) with certain concentration of HRP in a reaction volume of 1 mL acetate buffer (0.4 M, pH = 3.0) with 500 μmol/L TMB or ABTS as substrates were irradiated with a 300 W Xe lamp equipped with an ultraviolet cutoff filter ($\lambda \geq 400$ nm) to provide visible light source at room temperature.

The reaction kinetics for the catalytic oxidation of ABTS by the HRP-GO mixture was studied by monitoring the absorption intensity (for oxidized ABTS, oxABTS) at 417 nm with a 1 min interval under visible light irradiation. Catalytic experiments were carried out at 40 °C with 100 μL of GO and 0.08 mg/mL HRP in 1.0 mL acetate buffer (0.4 M, pH = 3.0) in the presence of varied concentrations of ABTS. The apparent kinetic parameters were calculated based on the Michaelis-Menten equation.

### 2.5. Colorimetric immunoassay of AFP based on the photo simulated activity of HRP by GO

Considering that the Au NPs are popular label tracers for various bioanalysis (Reza et al., 2018; Bahram et al., 2018; Ali et al., 2019), in this work, the Au NPs were prepared according to the previous method (Lin et al., 2011) and used as the label tracer. Briefly, 100 mL of 0.01% $HAuCl_4$ solution was heated to boil under vigorous stirring, followed by the quick addition of 2.5 mL of 1% trisodium citrate solution. The color of the reaction solution turned to wine red, indicating the formation of Au NPs. Followed by continued stirring and cooling down, the resulting Au NPs were stored in brown glass bottles at 4 °C ready for use. Subsequently, the detection antibody ($Ab_2$) and the capture DNA ($C_{DNA}$) were co-immobilized on the Au NPs for obtaining the Au NPs/$Ab_2$/$C_{DNA}$

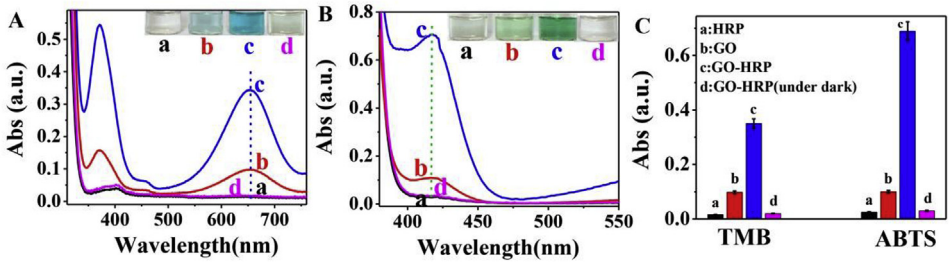


**Fig. 1.** The UV-Vis spectra of TMB (A) and ABTS (B) under different conditions: (a) HRP, (b) GO, and the mixture of GO and HRP are irradiated by the visible light (λ ≥ 400 nm) (c) or under dark conditions (d). Inset image is the corresponding color of the solutions. (C) The corresponding histogram of the absorption with different substrates. Irradiation time: 15 min, [GO] = 0.05 mg/mL, [HRP] = 0.08 mg/mL, pH = 3.0. (For interpretation of the references to color in this figure legend, the reader is referred to the Web version of this article.)

bioconjugates for signaling the immunoreaction. In detail, the bioconjugates were freshly prepared by gently mixing the $Ab_2$ (40 μL, 0.1 mg/mL) and 1.0 mL of the Au NPs solution for 2 h at room temperature. And then the thiolated $C_{DNA}$ activated by the tris (2-carboxyethyl) phosphine (TCEP) was added and allowed to react overnight at 4 °C. After blocking of the Au NPs by 200 μL of 1% BSA solution for 30 min at room temperature and centrifuging the mixture at 12,000 rpm for 30 min, the bioconjugates were washed by the washing buffer (20 mM phosphate buffer containing 0.1 M $NaClO_4$, pH 7.4), centrifuged again, and finally redispersed in 200 μL of 1% BSA for use.

The colorimetric immunoassay was conducted as follows: i) 20 μL of 0.1 mg/mL of the anti-AFP (capture antibody, $Ab_1$) was firstly spread onto the 96 well plates at 4 °C overnight, followed by rinsing with the washing buffer (20 mM phosphate buffer containing 0.1 M $NaClO_4$, pH 7.4) to remove the unabsorbed $Ab_1$. The coating of antibody on the polystyrene plate is through the adsorption effect resulted from the van der Waals forces between hydrophobic groups of the amino acid residues in the protein molecule (i.e., the antibody) and the polystyrene. Then, 25 μL of the 1% BSA blocking solution in 10 mM PBS containing 0.1 M KCl, 0.02% Tween-20 (pH 7.4) was introduced to block nonspecific binding sites for 2 h at 4 °C. ii) After thoroughly washing the plates with the washing buffer, 20 μL of different concentrations of the target antigen (Ag, that is, the AFP) was dropped in the wells and incubation for another 1 h. iii) After the immunoreaction between the $Ab_1$ and the Ag, the wells were allowed for labeling by an additional incubation with 25 μL of the Au NPs/$Ab_2$/$C_{DNA}$ bioconjugates' solution for 1 h and again washed thoroughly. iv) Subsequently, the mixture was incubated with 30 μL of the hairpin structured biotin-$H_1$ and biotin-$H_2$ (both was at the concentration of 1.0 mM) for 1 h at 37 °C to complete the HCR reaction. v) After washing three times with the washing buffer, the streptavidin labeled HRP (SA-HRP) was introduced and incubated for 1 h before washed thoroughly. Finally, 10 μL of 0.05 mg/mL GO, 100 μL of acetate buffer (pH = 3.0), and 20 μL of 5.0 mmol/L ABTS were sequentially added into the 96 well plates and illuminated for 15 min at 40 °C under visible light (λ ≥ 400 nm) irradiation. And the absorbance of oxABTS at 417 nm was measured.

## 3. Results and discussion

### 3.1. Manipulating the activity of HRP by the photo irradiated GO

Chemical oxidation of graphite by the Hummers' method has been proven to be a relatively mild, convenient, and effective means to produce GO with good dispersion in aqueous solutions (Li et al., 2008). As shown in the FT-IR spectrum of GO (Fig. S1A), the bands centered at 3400 $cm^{-1}$ and 1400 $cm^{-1}$ are attributed to the O–H stretching and vibration of the C–OH groups, respectively. While the peak at 1620 $cm^{-1}$ is attributed to C=C stretching vibrations and the C=O stretching of the –COOH is observed as the band at 1725 $cm^{-1}$. The band centered at 1098 $cm^{-1}$ is associated with the stretching of the C–O bond. All these vibrations are in accordance with the reported values of GO (Han et al., 2011; Stankovich et al., 2006). Raman spectroscopy (Fig. S1B) further confirms the successful preparation of GO: two characteristic peaks for GO at 1352 $cm^{-1}$, assigned to D band (the symmetry $A1_g$ mode), and at 1589 $cm^{-1}$, assigned to G band (the $E2_g$ mode of $sp^2$ carbon atoms) are observed (Liu et al., 2011). Moreover, the typical transmission electron microscopy (TEM) image of GO (Fig. S1C, insert) indicates its sheet-like morphology with occasional folds/wrinkles and rolled edges. The X-ray diffraction (XRD) pattern of the GO shows a typical diffraction peak at around 10.25° (Fig. S1C), corresponding to an interlayer spacing of 0.88 nm formed by the insertion of hydroxyl and epoxy groups between the graphite sheets (Yang et al., 2010).

Previously, we found that GO catalyzed the oxidation of the typical chromogenic substrate of HRP, i.e., TMB, under visible light irradiation (Wang et al., 2014). We now found that the existence of HRP can significantly augment the catalytic ability of the photo irradiated GO for the oxidation of the two substrates of HRP, i.e., ABTS and TMB (Fig. 1). The emergence of the characteristic absorption peaks at 370/652 nm and 417 nm for the oxidized TMB (oxTMB) and oxidized ABTS (oxABTS) accompanied by blue and green color development confirms that the oxidation products of TMB or ABTS by the HRP-GO mixture are the same as that of the conventional reactions catalyzed by the HRP using $H_2O_2$ as an initiator (Bos et al., 1981; Thiramanas et al., 2013). As a result, we attribute the above phenomenon to the activation of HRP by the illuminated GO because control experiments do not show obvious effect for the oxidation of TMB/ABTS by using the visible light irradiated HRP alone (Fig. 1, curve a). Likewise, there is no obvious oxidation effect for TMB/ABTS in the presence of GO and HRP under dark conditions (Fig. 1, curve d), hinting that both GO and visible light irradiation are all necessary for switching on the activity of HRP. In view of the extent of the catalytic oxidation effect, we chose ABTS as a typically chromogenic substrate to investigate the activation characteristics for HRP in the following experiments.

We compared the effects for the oxidation of ABTS under different concentrations of GO or $H_2O_2$ in the photoactivated GO-HRP and the conventional $H_2O_2$ initiated HRP (HRP-$H_2O_2$) systems. As show in Fig. S2, with the increased concentrations of GO or $H_2O_2$, the characteristic absorption peaks of the oxABTS at 417 nm raise gradually for the fixed concentration of HRP. The photoactivated GO-HRP system can reach higher oxidation extent (with the absorbance of 0.70) than the conventional $H_2O_2$-GO system (with the absorbance of 0.58). And we also find that the amount of GO and $H_2O_2$ in the similar concentration range produce similar degree of catalytic effect for the oxidation of the ABTS. This means that the photoactivated GO-HRP is relatively more efficient for the biocatalytic reaction.

As indicated in Fig. S3, similar to the conventional HRP based catalytic reaction system using $H_2O_2$ as an initiator, the photo triggered enzymatic activity of HRP by GO is also dependent on reaction temperature and solution pH. Though the GO mediated direct oxidization of ABTS system reaches its maximum catalytic activity at around the temperature of 30 °C and pH of 4.0, the optimal conditions for GO triggered HRP are found at 40 °C and pH of 3.0, respectively (Figs. S3A and B). At the fixed amount of GO, the as formed oxABTS in the system increases accompanied by an increased absorption intensity when the concentrations of the HRP increases (Fig. S3C) due to increased amount

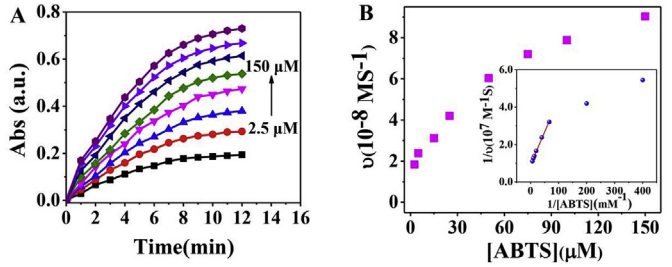


**Fig. 2.** (A) Absorbance of oxABTS at 417 nm versus time by GO-HRP with different concentrations of ABTS and (B) steady–state kinetic assay of GO-HRP as the photo biocatalyst illuminated under visible light irradiation (λ ≥ 400 nm). Insets are the Lineweaver–Burk plots of the double reciprocal of the Michaelis–Menten equation. Conditions: pH = 3.0, 40 °C. [GO] = 0.05 mg/mL, [HRP] = 0.08 mg/mL.

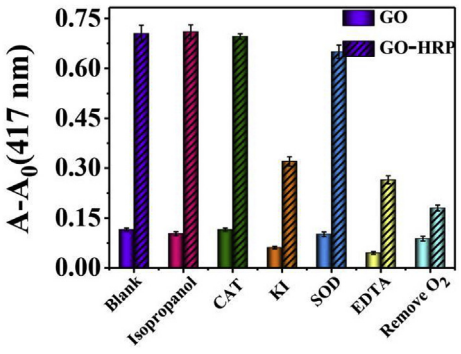


**Fig. 3.** Effects of different scavengers on the oxidation of ABTS by GO or GO-HRP under visible light irradiation. The error bars indicate relative standard deviation of four repeated experiments. [GO] = 0.05 mg/mL, [HRP] = 0.08 mg/mL, pH = 4.0, 30 °C (by GO); pH = 3.0, 40 °C (by GO-HRP).

of HRP available for activation. The catalytic oxidation of ABTS by the HRP-GO mixture proceeds relatively fast, which can reach the balance at around 20 min (Fig. S3D).

The steady-state kinetics study demonstrates typical Michaelis–Menten curves for the photochemical activity of HRP by GO with ABTS as the substrate in a certain range of concentrations (from 2.5 to 150 μM, Fig. 2A). The Michaelis–Menten constant ($K_m$), an indicator of enzyme affinity for its substrate, is obtained using Lineweaver–Burk plots (Fig. 2B, insert). The apparent kinetic parameters are calculated by the equation $\upsilon = V_{max} \times [S]/(K_m + [S])$, where υ is the initial enzymatic reaction rate, [S] is the concentration of the substrate, $V_{max}$ is the maximum enzymatic reaction rate and $K_m$ is the Michaelis-Menten constant. The apparent $K_m$ and $V_{max}$ value of GO-HRP with ABTS as substrate was 0.296 mmol/L and 108.1 nmol $L^{-1}$•$S^{-1}$, respectively. Distinctly, the $K_m$ value of GO-HRP with ABTS as a substrate is much lower than that of HRP ($K_m$ = 1.56 mmol/L) when using $H_2O_2$ as an initiator (Zhang et al., 2014), indicating that the photo triggered GO-HRP has a higher affinity for ABTS than that of HRP activated by $H_2O_2$.

Moreover, we investigated the stability of HRP against degradation during the performed irradiation times at pH of 3.0. Aliquots of this mixture were taken at regular time intervals and HRP activity was measured according to a conventionally standardized protocol by using TMB and $H_2O_2$ as the oxidizing reagent. It is found that no observable changes in HRP activity occur during the initial 25 min of reaction (Fig. S4). After longer reaction under the developed conditions, the activity of HRP is gradually reduced.

### 3.2. Mechanism of the activated HRP by the visible light irradiated GO

As opposed to the conventional iron containing catalytic center of the HRP is activated by $H_2O_2$ to catalyze the oxidation of different organic substrates (Tatsuma et al., 1994). Some reactive oxygen species (such as $O_2^{\bullet -}$ and hydroxyl radical ($^{\bullet}OH$)) (Fruk et al., 2007) and photo generated holes ($h^+$) (Kamada et al., 2011) were also found to trigger the catalytic activity of HRP. We employed an array of quenching agents to scavenge the relevant reactive species including hydroxyl radicals ($^{\bullet}OH$), superoxide anions ($O_2^{\bullet -}$) and photo-generated holes ($h^+$) in the catalytic system to certify the activation mechanism. As indicated in Fig. 3, variations in the catalytic activities in the presence of different scavengers are identical for the systems of GO and GO-HRP, indicating that the reactive species responsible for TMB oxidization are identical in both systems. The addition of isopropanol or catalase (CAT), i. e., the scavengers of $^{\bullet}OH$ and $H_2O_2$ (Hu et al., 2017), respectively, does not cause variation in the catalytic systems of GO and GO-HRP. On the contrary, when ethylene diamine tetraacetic acid (EDTA) disodium salt, KI (the scavenger for $h^+$) or superoxide dismutase (SOD, the scavenger for $O_2^{\bullet -}$) is introduced (Wang et al., 2012), the catalytic activities of GO and GO-HRP are distinctly inhibited, proving that the $h^+$ and $O_2^{\bullet -}$ are the main reactive species. Meanwhile, the catalytic activity of the system is inhibited when removing of dissolved oxygen, demonstrating that the catalytic reaction is indispensable of oxygen. In conclusion, though the photo irradiated GO can produce $h^+$ and $O_2^{\bullet -}$ for the direct oxidizing of ABTS, this catalytic activity was relatively low. On the contrary, the activated HRP by the $h^+$ and $O_2^{\bullet -}$ showed enhanced catalytic activity for the substrate oxidation.

What is more, we introduced photoelectrochemical experiments (Meng et al., 2013) to further confirm the origin of the production of the reactive species (i.e., $h^+$ and $O_2^{\bullet -}$) by GO. As illustrated in Fig. 4A, GO promptly generates stable and reproducible photocurrent with a reproducible response to the "on/off" visible light irradiation cycles, demonstrating the effective electron/hole generation and migration for the photo activated GO. For the structure of GO, the two dimensional (2D) carbon network of π-conjugated $sp^2$ (responsible for the conductivity) islands are surrounded by an insulating matrix of the $sp^3$ domains with oxygen-containing functional groups. Under photo-excitation, the electrons in its $sp^2$ domains are excited into the anti-bonding π (π*) orbital consisted conduction band (CB) and holes are created in the π orbital consisted valence band (VB). Then, the photo-generated electrons can capture dissolved oxygen from the CB of GO to produce $O_2^{\bullet -}$. This is because the CB potential (measured as −0.93 V versus saturated Ag/AgCl, Fig. 4B) of GO measured by the linear potential scans (Yeh et al., 2013) is more negative than that of the reduction potential of dissolved oxygen (−0.046 V versus normal hydrogen electrode (NHE)) (Chen et al., 2010). Both the photogenerated $O_2^{\bullet -}$ and $h^+$ can oxidize HRP to its oxidized state, which then oxidized the organic substrate accompanied by electron reduction of the oxidized state to the initial state.

Previous reports about the nanomaterials triggered HRP system using Amplex Ultrared (AUR) as the fluorescent substrate are inappropriate to attain a precise time and/or spatial resolution of the enzyme reaction because of the long lifetime of $O_2^{\bullet -}$ in neutral and basic solutions, leading to continued enzymatic reaction even after turning off the irradiation (Fruk et al., 2007). To study the controllability of the developed GO-HRP system, we measured the absorbance of oxABTS versus reaction time in an alternative dark and light environment (every 2 min) (Fig. 4C). When the light is switched on, there is immediate formation of the oxidation product, and hence, a simultaneous increase in the absorbance is observed. If the light is turned off, there is little oxidation products produced with little absorbance increment. Based on the fact, it can be concluded that the activity of HRP triggered by GO can be facilely and precisely switched by turning on/off the visible light. That is, it is appropriate to obtain a precise time resolution of the enzymatic reaction of HRP without the assistance of additional $H_2O_2$ and concentrated $H_2SO_4$. This is because in the acidic environment, the active intermediates, $O_2^{\bullet -}$ and $h^+$ have a short

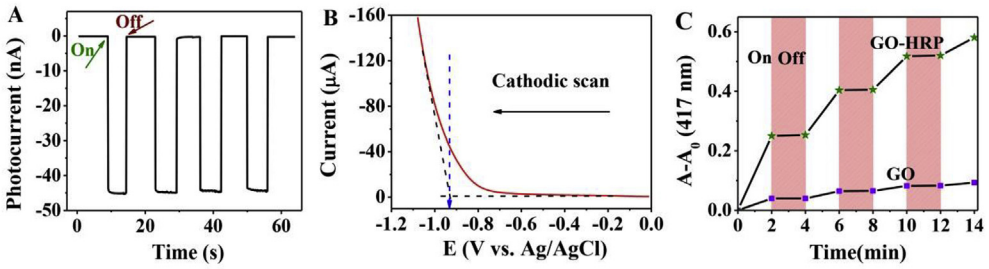


**Fig. 4.** (A) Photocurrent-time performances of GO modified indium tin oxide (ITO) electrode in 0.1 M $Na_2SO_4$ aqueous solution under visible light irradiation ($\lambda \geq 400$ nm). (B) Cathodic linear potential scan for determining the CB of the GO in the deaerated 0.1 M $Na_2SO_4$ aqueous solution. (C) Photoswitching behaviors of GO and GO-HRP for the catalytic oxidation of 0.5 mM ABTS under visible light irradiation.

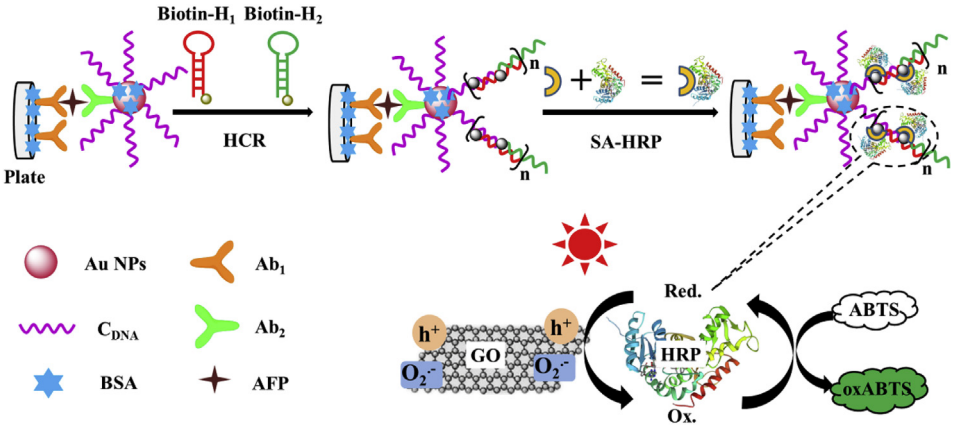


**Scheme 1.** Schematic illustration of the colorimetric sensing strategy for AFP amplified by HCR on the basis of the activated HRP by GO for signal readout.

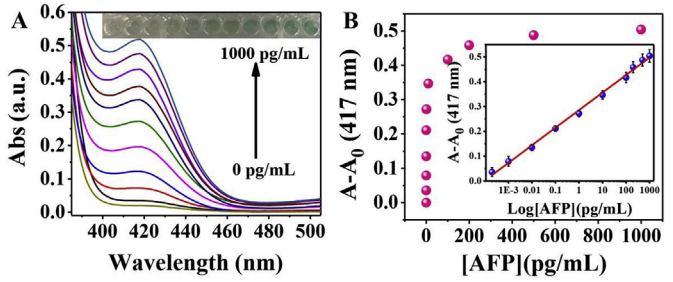


**Fig. 5.** (A) UV-Vis absorption spectra of the detection system in the presence of different concentrations of AFP (0, $2 \times 10^{-4}$, $1 \times 10^{-3}$, 0.01, 0.1, 1, 10, 100, 200, 500, 1000 pg/mL). Inset: the corresponding photographs of different solutions for detection. (B) The absorbance variation of oxABTS at 417 nm against AFP concentrations of the detection system. Inset: The linear calibration plots for AFP detection. Error bars represent the standard deviation of four repeated measurements.

lifetime (Kamada et al., 2012), and thus the enzymatic reaction stops rapidly after turning off the irradiation.

### 3.3. Colorimetric immunoassay of AFP based on the GO triggered HRP for signal readout

The applicability of the photo activated GO-HRP for biosensing was evaluated by immunoassay of AFP (taken as a model target), which was mainly based on the following reactions (shown in Scheme 1): i) The sandwich reaction between the capture antibody ($Ab_1$), the antigen (AFP) and the detection antibody ($Ab_2$) led to the fixing of the Au NPs/$Ab_2$/$C_{DNA}$ bioconjugates (i.e., the $Ab_2$ and the capture DNA ($C_{DNA}$) co-immobilized Au NPs) for signaling the immunoreaction (Scheme S1); ii) and then the hybridization chain reaction (HCR) reaction would happen (Zhang et al., 2012): the $C_{DNA}$ on the Au NPs as an initiator strand for the HCR reaction was opened by the biotin labeled hairpin probe $H_1$ (biotin-$H_1$) through hybridization and exposed the newly sticky end of the $H_1$ to open the biotin labeled hairpin probe $H_2$ (biotin-$H_2$) and exposed a newly sticky end on $H_2$ for repeated and extended hybridization. iii) Since the two hairpins, i.e., $H_1$ and $H_2$, were labeled with biotin, the streptavidin labeled HRP (SA-HRP) was connected on the HCR reaction enlarged strands through the biotin/streptavidin bioaffinity reaction, and the accumulated HRP would be photo activated by GO to oxidize ABTS for signal readout. To validate our design, the confirmation for the formation of the Au NPs/$Ab_2$/$C_{DNA}$ bioconjugates was done first. The Au NPs before and after modification with $Ab_2$ and the $C_{DNA}$ were monitored by the UV − vis absorption spectrometry (Fig. S5). As seen from curve a, an absorption peak at 520 nm is observed for the prepared Au NPs. After incubated with the $Ab_2$, the characteristic peak of $Ab_2$ at 275 nm appears (curve b), certifying the successful immobilization of $Ab_2$ on Au NPs. Finally, after incubation of $C_{DNA}$ with Au NPs/$Ab_2$ complex, the characteristic absorption peak at 260 nm (for DNA) is obviously enhanced, proving the successful fixation of $C_{DNA}$ and the formation of the Au NPs/$Ab_2$/$C_{DNA}$ bioconjugates.

### 3.4. Sensitivity

Under the optimum condition (Fig. S6), we monitored the analytical properties of the developed colorimetric immunoassay towards different concentrations of AFP standards. As seen from Fig. 5A, the absorbance of the oxABTS increases with the increased AFP concentrations. A linear relationship between the absorbance and AFP concentrations is achieved within the range of 0.2 fg/mL to 1.0 ng/mL (inset in Fig. 5B). The regression equation of the linear relationship can be fitted as $y = 0.07 \log[AFP] + 0.36$. The limit of detection (LOD) at a signal-to noise ratio of $3S_B$ (where $S_B$ is the standard deviations from the blank sample, n = 13) was estimated as 0.1 fg/mL. This detection limit is much lower than other assays for AFP detection proposed in literatures, such as photoelectrochemistry (Luo et al., 2019), electrochemistry (Qi et al., 2014), electrochemiluminescence (Zou et al., 2017; Lin et al., 2011; Liang et al., 2012) and colorimetry (Ren et al., 2018) with different amplification strategies (listed in Table 1).

**Table 1**
Comparison of the proposed strategy with other AFP detection methods.

| Method | Linear range (pg/mL) | LOD (pg/mL) | Ref. |
|---|---|---|---|
| Photoelectrochemistry | 10–$5.0 \times 10^4$ | 1.2 | Luo et al. (2019) |
| Electrochemistry | 10–$1.2 \times 10^4$ | 5.0 | Qi et al. (2014) |
| ECL[a] | 0.05–100 | 0.01 | Zou et al. (2017) |
| ECL[a] | 0.01–$1.0 \times 10^3$ | $1.0 \times 10^{-3}$ | Lin et al. (2011) |
| ECL[a] | 10–$8.0 \times 10^4$ | 5.0 | Liang et al. (2012) |
| Colorimetry | 10–$1.0 \times 10^3$ | 2.3 | Ren et al. (2018) |
| Colorimetry | $2.0 \times 10^{-4}$–$1.0 \times 10^3$ | $1.0 \times 10^{-4}$ | (This work) |

[a] ECL: Electrochemiluminescence.

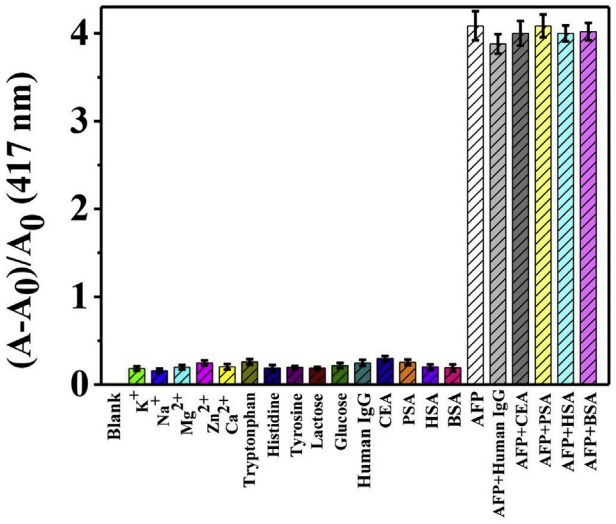


**Fig. 6.** The selectivity of the method towards AFP. The concentration of each substance was as follows: $K^+$, $Na^+$, $Mg^{2+}$, $Zn^{2+}$, $Ca^{2+}$, tryptonphan, histidine, tyrosine, lactose, and glucose were $1.0 \times 10^{-4}$ M; human IgG, carcinoembryonic antigen (CEA), human serum albumin (HSA), bovine serum albumin (BSA) and prostate-specific antigen (PSA) were 10 ng/mL; and the concentration of AFP was 0.1 ng/mL. Error bars represent the standard deviation of four repeated measurements.

### 3.5. Specificity and feasibility

The specificity of the proposed immunoassay was evaluated by challenging the immunosensor toward various potential interfering substances, such as metal ions, amino acids and other proteins. From Fig. 6, we can see that none of the tested substances causes obvious absorbance signal except for the target of AFP, which clearly demonstrates that the developed method has a good selectivity for AFP detection. The feasibility of the immunoassay system for potential real sample detections was investigated using human serum. The results in Table S1 display that they agree well with that of the commercially available enzyme-linked immunosorbent assay (ELISA) kits, with relative errors less than 10%, indicating acceptable accuracy of the proposed protocol for real sample detections.

## 4. Conclusion

The present study demonstrates that the visible light irradiated GO can trigger the enzymatic activity of HRP for the conversion of its typical chromogenic substrates (including TMB and ABTS). This photoswitched enzymatic reaction can be easily realized by turning on or off the visible light irradiation, which is considered to be a prominent technique in view of the fact that it requires no initiator (peroxide) or terminator (strongly acidic solution) and is effective for time precise control. Furthermore, the photoswitchable GO-HRP has been proven to be an efficiently catalytic label tracer for the immunoassay of the AFP (taken as a model analyte) with high performances in terms of sensitivity and selectivity. Thus, the proposed photoswitchable hybrid that associating prominent substrate/reaction selectivity of enzymes with photocontrollability of activity, may find various applications in biosensors and catalysis in future.

## CRediT authorship contribution statement

**Genxia Cao:** Investigation. **Dongxue Sun:** Writing - original draft. **Tiantian Gu:** Resources. **Yuming Dong:** Validation. **Guang-Li Wang:** Funding acquisition, Project administration, Supervision.

## Declaration of competing interest

The authors declare that they have no known competing financial interests or personal relationships that could have appeared to influence the work reported in this paper.

## Acknowledgement

This work was supported by the National Natural Science Foundation of China (Grants 21575052, 21676123), the MOE & SAFEA for the 111 Project (B13025), the Fundamental Research Funds for the Central Universities (JUSRP21936) and the National First-class Discipline Program of Food Science and Technology (JUFSTR20180301).

## Appendix A. Supplementary data

Supplementary data to this article can be found online at https://doi.org/10.1016/j.bios.2019.111707.

## References

Ali, A., Mehdi, K., Bahram, A., Azam, N., Asghar, N., Leila, H., Jamal, R., Hamid, K., Narges, E., 2019. Int. J. Biol. Macromol. 124, 1256–1263.
Asghar, N., Melina, R., Bagher, F., Parvaneh, D., Javad, M., Bahram, A., Soheila, R., Nouraddin, A.G., 2019. Drug Dev. Res. 80, 402–424.
Bahram, A., Mehdi, K., Mojtaba, S., Parichehreh, Y., 2018. Spectrochim. Acta A 199, 421–429.
Bos, E.S., Doelen, A.A., Rooy, N.V., Schuurs, A.H., 1981. J. Immunoass. Immunochem. 2, 187–204.
Bretschneider, J., Reismann, M., Plessen, G., Simon, U., 2010. Small 5, 2549–2553.
Chen, C., Ma, W., Zhao, J., 2010. Chem. Soc. Rev. 39, 4206–4219.
Chen, L.C., Teng, C.Y., Lin, C.Y., Chang, H.Y., Chen, S.J., Teng, H., 2016. Adv. Energy Mater. 6, 1600719.
Chung, C., Kim, Y.K., Shin, D., Ryoo, S.R., Hong, B., Min, D.H., 2013. Acc. Chem. Res. 46, 2211–2224.
Fruk, L., Rajendran, V., Spengler, M., Niemeyer, C., 2007. ChemBioChem 8 2195– 2198.
Han, D., Yan, L., Chen, W., Li, W., 2011. Carbohydr. Polym. 83, 653–658.
Hu, H., Zhang, J., Ding, Y., Zhang, X., Xu, K., Hou, X., Wu, P., 2017. Anal. Chem. 89, 5101–5106.
Hummers, W., Offeman, R., 1958. J. Am. Chem. Soc. 80 1339 − 1339.
Hsu, H.C., Shown, I., Wei, H.Y., Chang, Y.C., Du, H.Y., Lin, Y.G., Tseng, C.A., Wang, C.H., Chen, L.C., Lin, Y.C., Chen, K.H., 2013. Nanoscale 5, 262–268.
Kamada, K., Nakamura, T., Tsukahara, S., 2011. Chem. Mater. 23, 2968–2972.
Kamada, K., Moriyasu, A., Soh, N., 2012. J. Phys. Chem. C 116, 20694–20699.
Krishnamoorthy, K., Mohan, R., Kim, S., 2011. Appl. Phys. Lett. 98, 244101.
Kuwabata, S., Nishida, K., Tsuda, R., Inoue, H., Yoneyama, H., 1994. J. Electrochem. Soc.

141, 1498–1503.
Li, D., Müller, M., Gilje, S., Kaner, R., Wallace, G., 2008. Nat. Nanotechnol. 2008 3, 101–105.
Li, P., Cao, G.X., Liu, Q.Y., Guo, Y.Y., Dong, Y., Li, Z., 2018. Sens. Actuators B Chem. 262, 110–117.
Liang, G., Liu, S., Zou, G., Zhang, X., 2012. Anal. Chem. 84, 10645–10649.
Lin, D., Wu, J., Yan, F., Deng, S., Ju, H., 2011. Anal. Chem. 83, 5214–5221.
Liu, K.P., Zhang, J.J., Cheng, F.F., Zheng, T.T., Wang, C.M., Zhu, J.J., 2011. J. Mater. Chem. 21, 12034–12040.
Luo, Z., Qi, Q., Zhang, L., Zeng, R., Su, L., Tang, D., 2019. Anal. Chem. 91, 4149–4156.
Meng, F., Li, J., Cushing, S.K., Zhi, M., Wu, N., 2013. J. Am. Chem. Soc. 135, 10286–10289.
Peng, J., Weng, J., 2017. Biosens. Bioelectron. 89, 652–658.
Qi, T., Liao, J., Li, Y., Peng, J., Li, W., Chu, B., Li, H., Wei, Y., Qian, Z., 2014. Biosens. Bioelectron. 61, 245–250.
Ren, R., Cai, G., Yu, Z., Zeng, Y., Tang, D., 2018. Anal. Chem. 90, 11099–11105.
Reza, S., Mojtaba, S., Bahram, A., Ahmad, J., Ebrahim, N., Ali, A., Arash, S., 2018. Mol. Cell. Probes 41, 8–13.
Song, Y.Y., Hildebrand, H., Schmuki, P., 2009. Electrochem. Commun. 11, 1429–1433.
Stankovich, S., Piner, R., Nguyen, S., Ruoff, R., 2006. Carbon 44, 3342–3347.
Tatsuma, A., Watanabe, T., Tatsuma, S., Watanabe, T., 1994. Anal. Chem. 66, 290–294.
Thiramanas, R., Jangpatarapongsa, K., Tangboriboonrat, P., Polpanich, D., 2013. Anal. Chem. 85, 5996–6002.
Wang, G.L., Li, X.Q., Cao, G.X., Yuan, F., Dong, Y., Li, Z., 2017. Chem. Commun. 53, 11165–11168.
Wang, G.L., Xu, X., Wu, X., Cao, G., Dong, Y., Li, Z., 2014. J. Phys. Chem. C 118, 28109–28117.
Wang, W., Jiang, X., Chen, K., 2012. Chem. Commun. 48, 7289–7291.
Wen, F., Dong, Y., Feng, L., Wang, S., Zhang, S., Zhang, X., 2011. Anal. Chem. 83, 1193–1196.
Xianyu, Y., Chen, Y., Jiang, X., 2015. Anal. Chem. 87, 10688–10692.
Yeh, T.F., Syu, J.M., Cheng, C., Chang, T.H., Teng, H., 2010. Adv. Funct. Mater. 20, 2255–2262.
Yeh, T.F., Chan, F.F., Hsieh, C.T., Teng, H., 2011. J. Phys. Chem. C 115, 22587–22597.
Yeh, T.F., Chen, S.J., Yeh, C.S., Teng, H., 2013. J. Phys. Chem. C 117, 6516–6524.
Yang, X.M., Tu, Y.F., Li, L., Shang, S.M., Tao, X.M., 2010. ACS Appl. Mater. Interfaces 2, 1707–1713.
Zhang, B., Liu, B., Tang, D., Niessner, R., Chen, G., Knopp, D., 2012. Anal. Chem. 84, 5392–5399.
Zhang, W., Ma, D., Du, J., 2014. Talanta 120, 362–367.
Zhang, Y., Tang, Z., Wang, J., Wu, H., Maham, A., Lin, Y., 2010. Anal. Chem. 82, 6440–6446.
Zou, G., Tan, O., Long, X., He, Y., Miao, W., 2017. Anal. Chem. 89, 13024–13029.